NRL Report 8333

Angle-of-Arrival Estimation Error for Shipboard Monopulse Radars

B. H. CANTRELL

Radar Analysis Staff
Radar Division

September 12, 1979

NAVAL RESEARCH LABORATORY
Washington, D.C.

SECURITY CLASSIFICATION OF THIS PAGE *(When Data Entered)*

REPORT DOCUMENTATION PAGE

READ INSTRUCTIONS BEFORE COMPLETING FORM

1. REPORT NUMBER: NRL Report 8333	2. GOVT ACCESSION NO. / 3. RECIPIENT'S CATALOG NUMBER
4. TITLE *(and Subtitle)*: ANGLE-OF-ARRIVAL ESTIMATION ERROR FOR SHIPBOARD MONOPULSE RADARS	5. TYPE OF REPORT & PERIOD COVERED: Interim report on a continuing NRL Problem
	6. PERFORMING ORG. REPORT NUMBER
7. AUTHOR(s): B. H. Cantrell	8. CONTRACT OR GRANT NUMBER(s)
9. PERFORMING ORGANIZATION NAME AND ADDRESS: Naval Research Laboratory, Washington, DC 20375	10. PROGRAM ELEMENT, PROJECT, TASK AREA & WORK UNIT NUMBERS: NRL Problem R02-97, Program Element 61153N-21, Project RR021-05-41
11. CONTROLLING OFFICE NAME AND ADDRESS: Department of the Navy, Office of Naval Research, Arlington, VA 22217	12. REPORT DATE: September 12, 1979
	13. NUMBER OF PAGES: 26
14. MONITORING AGENCY NAME & ADDRESS*(if different from Controlling Office)*	15. SECURITY CLASS. *(of this report)*: UNCLASSIFIED
	15a. DECLASSIFICATION/DOWNGRADING SCHEDULE

16. DISTRIBUTION STATEMENT *(of this Report)*

Approved for public release; distribution unlimited.

17. DISTRIBUTION STATEMENT *(of the abstract entered in Block 20, if different from Report)*

18. SUPPLEMENTARY NOTES

19. KEY WORDS *(Continue on reverse side if necessary and identify by block number)*

Monopulse radar
Angle estimates
Measurements

20. ABSTRACT *(Continue on reverse side if necessary and identify by block number)*

Angle estimates by shipboard monopulse radars are corrupted by sea-reflected multipath. It is shown that even though the elevation and azimuth estimates in antenna coordinates are badly corrupted for conditions of crosslevel and sea-reflected multipath, the azimuth error in the plane of the sea may be tolerable. The azimuth errors in the plane of the sea are often less than 0.1 beamwidth. The errors were studied under a variety of conditions, and the effect of scanning off axis as in a phased array was also included.

DD FORM 1 JAN 73 1473 EDITION OF 1 NOV 65 IS OBSOLETE
S/N 0102-014-6601

SECURITY CLASSIFICATION OF THIS PAGE *(When Data Entered)*

CONTENTS

INTRODUCTION 1

SIMULATION EQUATIONS 1

Coordinate Transforms 1
Monopulse Signals 4
Angle Estimation 5
Simulation Data Flow 6

SIMULATION RESULTS 6

ERRORS DUE TO THERMAL NOISE 17

SUMMARY 21

APPENDIX A — Reflection Coefficient 22

APPENDIX B — Coefficients for Covariance Calculations 24

ANGLE-OF-ARRIVAL ESTIMATION ERROR FOR SHIPBOARD MONOPULSE RADARS

INTRODUCTION

This report is concerned with the accuracy in the measurement of the angle of arrival of a received echo by an unstabilized monopulse radar in the presence of sea-reflected multipath. Specifically the azimuth and elevation angular errors in the plane of the sea as a function of a number of parameters are shown. The goal of the study is to demonstrate that even though the monopulse-radar errors are large along the principal antenna axis under ship roll and pitch and sea-reflected multipath conditions, the azimuth error in the plane of the sea is not too large.

A UHF phased-array radar is used as the vehicle for showing the results. The outline of the basic steps for obtaining the results are as follows. The target and image location are given in the plane of the sea. These coordinates are transformed to the antenna coordinates where the antenna is located on a rolled and pitched ship. The monopulse radar signals are formed, and the azimuth and elevation angles in antenna coordinates are found. This location is transformed back into the plane of sea and compared to the original given location. In addition the errors due to thermal noise are studied.

SIMULATION EQUATIONS

The equations used in the simulation are outlined in this section. To begin, the location of objects in the plane of the sea are related to antenna coordinates.

Coordinate Transforms

The Cartesian coordinate system in deck coordinates (x_d, y_d, z_d) is defined such that the y_d axis lies along the deck of the ship in the aft-to-bow direction and the z_d axis is perpendicular to the deck of the ship. The gimbals of the gyro are set so that the roll axis is attached to the ship and the pitch axis is attached to the roll platform. The roll is positive when the deck is down on the port side, and the pitch is positive when the bow is down. The relation between the stabilized coordinates and the deck coordinates is obtained through two rotations and is

$$\begin{bmatrix} x_s \\ y_s \\ z_s \end{bmatrix} = T \begin{bmatrix} x_d \\ y_d \\ z_d \end{bmatrix} \tag{1}$$

Manuscript submitted May 23, 1979.

or

$$\begin{bmatrix} x_d \\ y_d \\ z_d \end{bmatrix} = T^t \begin{bmatrix} x_s \\ y_s \\ z_s \end{bmatrix}, \tag{2}$$

where T^t is the transpose of T:

$$T = \begin{bmatrix} \cos R & 0 & -\sin R \\ \sin R \sin P & \cos P & \cos R \sin P \\ \sin R \cos P & -\sin P & \cos R \cos P \end{bmatrix}, \tag{3}$$

in which R and P are the roll and pitch angles respectively. The Cartesian coordinates are related to the polar coordinates by

$$x_s = r \cos e_s \sin a_s, \tag{4}$$

$$y_s = r \cos e_s \cos a_s, \tag{5}$$

and

$$z_s = r \sin e_s \tag{6}$$

and conversely by

$$a_s = \tan^{-1} x_s/y_s \tag{7}$$

and

$$e_s = \sin^{-1} z_s/r, \tag{8}$$

where a_s, e_s, and r are the azimuth, elevation, and range in the plane of the sea.

It is desirable to measure azimuth from the array face rather from the bow of the ship, assuming the antenna lies in the $x_d z_d$ plane before being rotated on tilted. Then, if the antenna is rotated about the z_d axis by an angle $\mathcal{A}$, the deck coordinates are transformed to face coordinates. If in addition the array is tilted back by an angle $\mathcal{B}$, the coordinates must be rotated about the x axis. The new face-coordinate system (x_f, y_f, z_f) has the y_f axis normal to the array, and the array lies in the $x_f z_f$ plane. The relation between the coordinates is

$$\begin{bmatrix} x_d \\ y_d \\ z_d \end{bmatrix} = W \begin{bmatrix} x_f \\ y_f \\ z_f \end{bmatrix}, \tag{9}$$

where $W\,W^t = I$ and

$$W = \begin{bmatrix} \cos\mathscr{A} & \sin\mathscr{A}\cos\mathscr{B} & -\sin\mathscr{A}\sin\mathscr{B} \\ -\sin\mathscr{A} & \cos\mathscr{A}\cos\mathscr{B} & -\cos\mathscr{A}\sin\mathscr{B} \\ 0 & \sin\mathscr{B} & \cos\mathscr{B} \end{bmatrix}. \tag{10}$$

The stabilized coordinates and face coordinates are then related by

$$\begin{bmatrix} x_s \\ y_s \\ z_s \end{bmatrix} = TW \begin{bmatrix} x_f \\ y_f \\ z_f \end{bmatrix} \tag{11}$$

and

$$\begin{bmatrix} x_f \\ y_f \\ z_f \end{bmatrix} = W^t T^t \begin{bmatrix} x_s \\ y_s \\ z_s \end{bmatrix}. \tag{12}$$

The array coordinates in azimuth and elevation, denoted by γ and δ respectively, are

$$\gamma = \sin^{-1}(x_f/r) \tag{13}$$

and

$$\delta = \sin^{-1}(z_f/r) \tag{14}$$

or conversely as

$$x_f = r\sin\gamma, \tag{15}$$

$$z_f = r\sqrt{\cos^2\delta - \sin^2\gamma}, \tag{16}$$

and

$$z_f = r\sin\delta. \tag{17}$$

Equations (13) through (17) incorporate the coning (scanning off axis) present in antennas, and the antenna azimuth γ should not be construed to be the same as the azimuth a_f in the coordinates on the face of the array, which is

$$a_f = \sin^{-1}\frac{x_f}{\sqrt{x_f^2 + y_f^2}}. \tag{18}$$

The use of the coordinate conversions is described as follows. The target and image location is specified in the plane of the sea. Equations (12), (13), and (14) are used to define the target and image in array coordinates, which are used in determining the monopulse signals. After the angle of arrival is estimated in antenna coordinates by monopulse techniques, equations (11), (15), (16), (17), (7), and (8) are used to obtain the angle of arrival in the plane of the sea.

Monopulse Signals

An amplitude-comparison monopulse is used in this study. Consequently the phase of any plane wave will be the same for the sum and the two difference signals but differ in magnitude by the gain of the antenna pattern in the direction of the received signal. The three monopulse signals are given by the sum of the direct signal and the reflected signal caused by the reflecting sea surface, as shown in Fig. 1. The equations describing the signals are

$$\Sigma = AG_{\Sigma}[(\gamma_T - \gamma_P), (\delta_T - \delta_P)]e^{j\theta} + \rho AG_{\Sigma}[(\gamma_I - \gamma_p), (\delta_I - \delta_p)]e^{-j\theta}, \tag{19}$$

$$\Delta_{\gamma} = AH_{\gamma}[(\gamma_T - \gamma_P), (\delta_T - \delta_P)]e^{j\theta} + \rho AH_{\gamma}[(\gamma_I - \gamma_p), (\delta_I - \delta_p)]e^{-j\theta}, \tag{20}$$

and

$$\Delta_{\delta} = AH_{\delta}[(\gamma_T - \gamma_p), (\delta_T - \delta_p)]e^{j\theta} + \rho AH_{\delta}[(\gamma_I - \gamma_p), (\delta_I - \delta_p)]e^{-j\theta}, \tag{21}$$

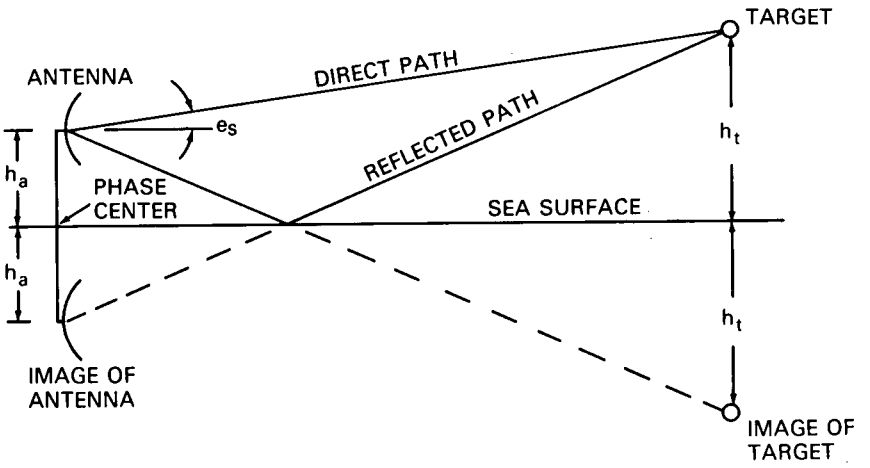

Fig. 1 — Multipath-propagation geometry

where Σ, Δ_{γ}, and Δ_{δ} are the sum and the two difference signals in azimuth and elevation, γ_T and δ_T are the target azimuth and elevation in antenna coordinates, γ_I and δ_I are the image azimuth and elevation in antenna coordinates, γ_p and δ_p are the pointing

azimuth and elevation angles, A is the complex amplitude of the signal, ρ is the complex reflection coefficient, G_Σ, H_γ, and H_δ are the antenna patterns for the sum and the difference patterns in azimuth and elevation, and θ is 1/2 the phase shift of the reflected signal from the direct signal due to path difference. The value of θ is approximately

$$\theta = 2\pi h_a e_s/\lambda, \tag{22}$$

where (Fig. 1) h_a is the antenna height, e_s is the target elevation in stabilized coordinates, and λ is the wavelength. The computation of the complex reflection coefficient ρ is described in Appendix A and is valid for only a smooth sea. The antenna patterns used in this simulation are

$$G_\Sigma(\alpha, \beta) = \left[\frac{\sin \pi d\alpha/\lambda}{\pi d\alpha/\lambda} \frac{\pi^2}{\pi^2 - (\pi d\alpha/\lambda)^2}\right] \frac{\sin \pi D\,\beta/\lambda}{\pi D\beta/\lambda}, \tag{23}$$

$$H_\gamma(\alpha, \beta) = \frac{\pi \sin \pi d\alpha/\lambda}{\pi^2 - (\pi d\alpha/\lambda)^2} \frac{\sin \pi D\beta/\lambda}{\pi D\beta/\lambda}, \tag{24}$$

and

$$H_\delta(\alpha, \beta) = \left[\frac{\sin \pi d\alpha/\lambda}{\pi d\alpha/\lambda} \frac{\pi^2}{\pi^2 - (\pi d\alpha/\lambda)^2}\right] \frac{1 - \cos \pi D\beta/\lambda}{\pi D\beta/\lambda}, \tag{25}$$

where α and β are dummy parameters representing azimuth and elevation respectively and d and D are the array dimensions. Equations (19) and (20) were not used in the exact form given but were modified to account for polarization changes of the array with respect to the plane of the sea under crosslevel conditions. The modification is given in Appendix A along with the discussion of the reflection coefficient.

Angle Estimation

The monopulse performs the operation

$$R_\gamma = \Sigma^* \Delta_\gamma / \Sigma^* \Sigma \tag{26}$$

and

$$R_\delta = \Sigma^* \Delta_\delta / \Sigma^* \Sigma \tag{27}$$

to obtain signals R_γ and R_δ, which are related to the azimuth and elevation of a plane wave. The relation can be found in closed form in the present case by momentarily letting ρ equal zero, so a plane-wave condition is formed, and placing (19), (20), and (21) into (26) and (27), which yields

$$R_\gamma = H_\gamma/G_\Sigma = \frac{2d}{\lambda}\,\gamma_T \tag{28}$$

and

$$R_\delta = H_\delta / G_\Sigma = \frac{D\pi}{2\lambda} \tan \delta_T. \tag{29}$$

The estimate of the target position, even though multipath is present, is

$$\hat{\gamma}_T = \frac{\lambda}{2d} R_\gamma \tag{30}$$

and

$$\hat{\delta}_T = \frac{2\lambda}{D\pi} \tan^{-1} R_\delta. \tag{31}$$

Simulation Data Flow

The basic data flow of the simulation is given in Fig. 2. The target, image, and beam-pointing angles are defined in the plane of the sea. By coordinate transforms the target, image, and beam-pointing angles are represented in terms of antenna coordinates. The monopulse signals using equations (19) through (21) are formed with the aid of the multipath model. The azimuth and elevation are estimated using standard monopulse techniques and in the present case by equations (26), (27), (30), and (31). The estimated azimuth and elevation angles given in antenna coordinates are transformed back to the plane of the sea. The final step is to subtract the estimated and true azimuth and elevation angles in the plane of sea and plot the error.

SIMULATION RESULTS

An extensive set of error curves were run for this study. However, only a representative set of the curves, will be shown and discussed. Some of the general conclusions are drawn from the larger set of data not shown.

In all the figures to be shown (Figs. 4 through 9) $\mathscr{A} = 90°$ and $\mathscr{B} = 0°$, which means the antenna is pointed directly out from and perpendicular to the starboard side. Consequently, with no roll the pitch angle is the crosslevel angle of the array, and with no pitch the roll angle is the level angle of the array. The errors are plotted only within the half-power contours of the beams. The errors in two beam positions per figure are shown. The even-number figures have the beam-elevation pointing angle in the plane of the sea coordinates of 1/2 beamwidth and 3/2 beamwidths above the plane of the sea. The odd-number figures have the beam-elevation pointing angle in the plane of the sea coordinates of 0 and 1 beamwidth above the plane of the sea. Each figure has four parts: the azimuth error for horizontal polarization, the elevation error for horizontal polarization, the azimuth error for vertical polarization, and the elevation error for vertical polarization. The error is plotted as a function of target elevation with a fixed azimuth with these coordinates taken in the plane of the sea.

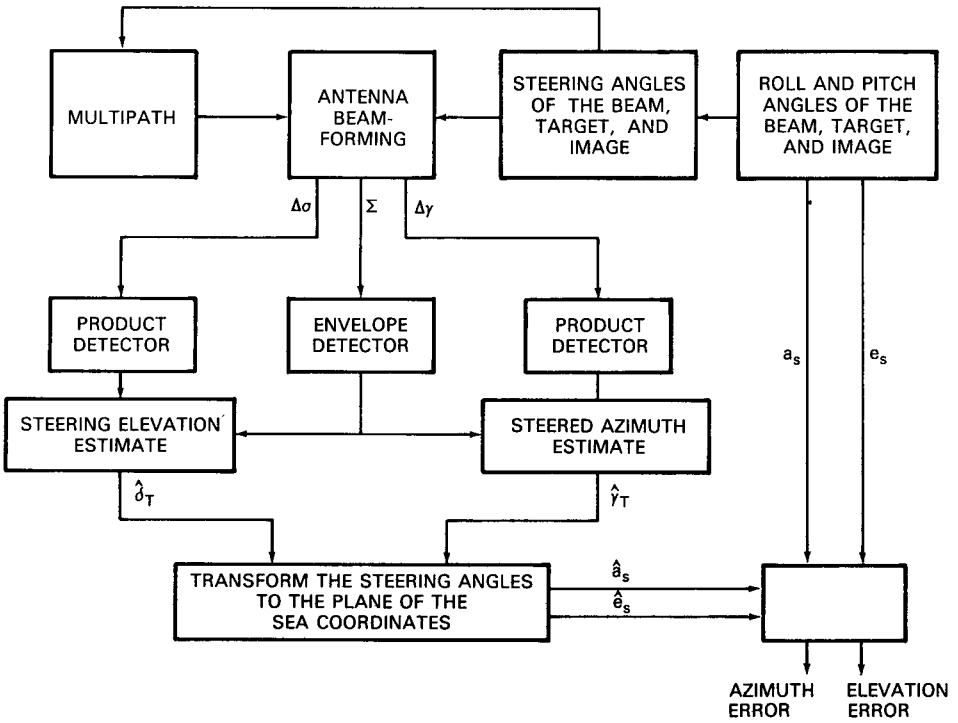

Fig. 2 — Simulation

Figure 3 may be helpful in visualizing the geometry of problem. Figure 3a shows the 3-dB contours for two beam positions of the elevation pointing angle of 1/2 and 3/2 beamwidths off the sea surface, and the azimuth is set such that no beam steering off boresite is necessary in the azimuth plane. The roll and pitch are zero. The locus of target positions is for a fixed azimuth of 88° and the elevation in the plane of the sea is varied. Figure 3b shows the same situation as Fig. 3a except for two differences. The pitch is nonzero, causing crosslevel changes in the beam, and the beam-pointing angles in elevation are now 0 and 1 beamwidth for the two beams. Figure 3c is the same as Fig. 3a except that the beam is scanned off axis to the left and azimuth in the locus of target positions is moved over by the same amount.

To initiate discussion of the noise-free case (consideration of bias errors), Figs. 4 and 5 are referred to. In these figures the beam is not scanned off axis in azimuth and there is no crosslevel. The most striking results in these figures is that there is no azimuth error, because there is no coupling between azimuth and elevation for this condition and all the monopulse error is in the elevation angle. In general the errors in elevation are large. Vertically polarized antennas typically yield less error than horizontally polarized ones due to the lower reflection coefficient for a smooth reflecting sea. The errors are nonzero in the upper beam positions because of the antenna sidelobes. When the target and image are in phase, the elevation estimate is between the target and image, or near the sea surface, denoted on the figures by positive elevation error; and the target and image are nearly out of phase, the elevation is much higher than the strongest target, denoted by negative elevation error. This is most

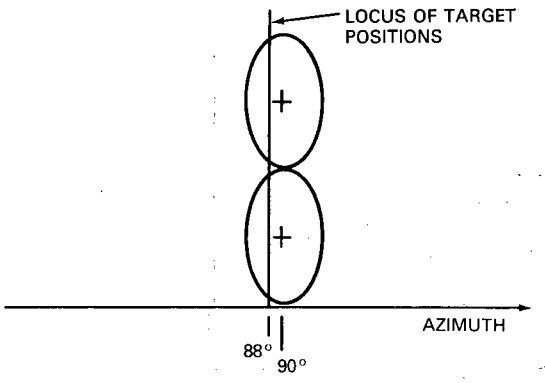

(a) Roll angle R = 0, pitch angle P = 0, $\mathscr{A}$ = 90°, $\mathscr{B}$ = 0, pointing azimuth a_p = 90°, and pointing elevations e_p = 1/2 and 3/2 beamwidths

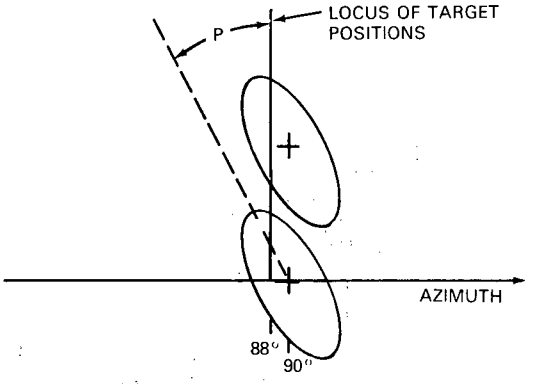

(b) R = 0, P = 20°, $\mathscr{A}$ = 90°, $\mathscr{B}$ = 0, a_p = 0, and e_p = 0 and 1 beamwidth

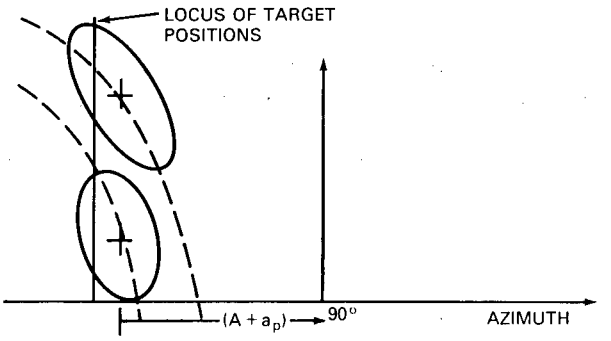

(c) R = 0, P = 0, $\mathscr{A}$ = 90°, $\mathscr{B}$ = 0, a_p = 45°, and e_p = 1/2 and 3/2 beamwidths

Fig. 3 — Typical locus of target positions used for plotting errors

prominent in Fig. 5b, because the target and image are essentially the same value. The angle estimate is at the sea surface except when the multipath null is on the antenna, which yielded very large negative spike errors. The spike errors are not as large on the figure as they should be, because not fine enough quantization was used in the target elevation.

Figures 6 and 7 show the errors when the array is crossleveled by 20°, which in this case corresponds to a roll of 0° and a pitch of 20°. Because of the crosslevel both the array azimuth and elevation measurements are corrupted by the image. However, when the measurement is transformed back into the plane of the sea, the azimuth errors seemed tolerable. For vertical polarization with the beam pulled up (Fig. 6c) the maximum error is about 0.05 beamwidth, and for horizontal polarization (Fig. 6a) the maximum error is about 0.1 beamwidth. When the beam was centered on the horizon (beam 1 in Fig. 7), the azimuth error was nearly zero unless the multipath null or minimum was on the array, in which case the errors were large. The elevation errors are somewhat smaller with crosslevel than without crosslevel, because the image signal strength is reduced in magnitude from the target due to the beam shape.

Figures 8 and 9 show the errors when the array is scanned off axis (coned) by 45°. Because of the coning the elevation errors corrupt the azimuth measurements in the plane of sea. The errors in Fig. 8a were some of the largest azimuth errors found in the study except when the elevation beamwidth became small for nearly the same conditions as in Fig. 8a. Then the coning-induced errors became large.

Examples of the errors induced by crosslevel changes and scanning off axis were given. These are the two basic mechanisms for coupling errors induced by sea-reflected multipath into the azimuth measurement in the plane of sea. The effects of varying other parameters will be briefly discussed (without showing the error curves on which the discussions are based).

Level changes on the array with respect to the plane of the sea were investigated. The beam-pointing angle could be changed by ship motion (roll and pitch) or by changing the mounting of the array on the ship. In all cases the beam was electronically steered to obtain the correct beam-pointing angle in the plane of the sea. The result is that essentially no changes occurred in the azimuth and elevation errors over many different conditions. The level changes investigated were between $-20°$ and $20°$. However, these results probably hold for values considerably in excess of $\pm 20°$.

The effect on the azimuth errors of the target position in azimuth (which of course must be within a 3-dB beamwidth) is fairly small. The largest changes are due to crosslevel, primarily because the effective reflection coefficient of the image, which coefficient includes the beam shape, is modified slightly.

The effect of a change in antenna height on an error curve is to cause the errors to oscillate up and down at a different rate but retain the same error envelope. A change in frequency primarily gives the same result except that the envelope of the errors is modified slightly in the case of vertical polarization.

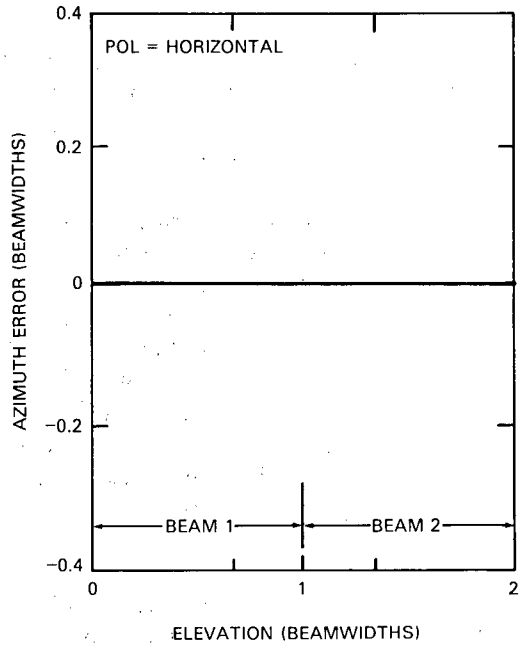

(a) Horizontal polarization

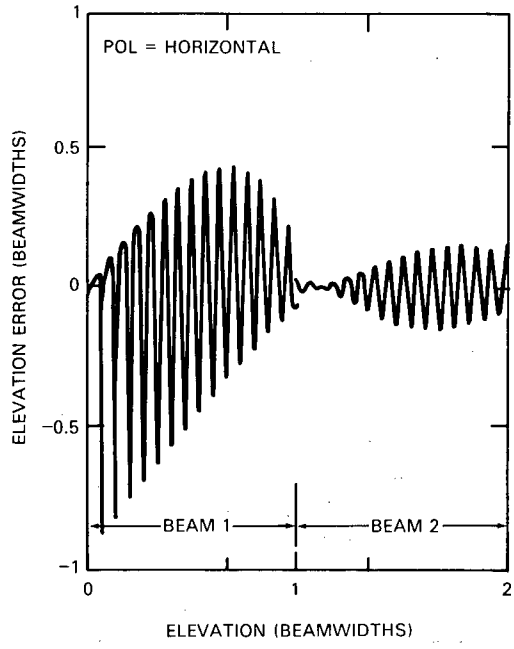

(b) Horizontal polarization

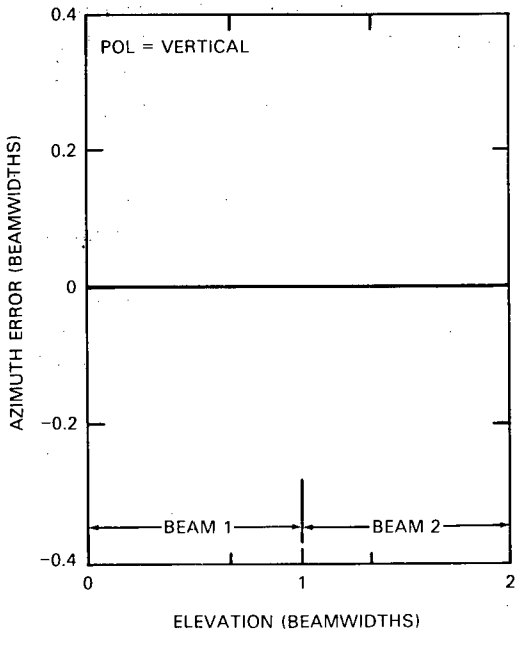

(c) Vertical polarization

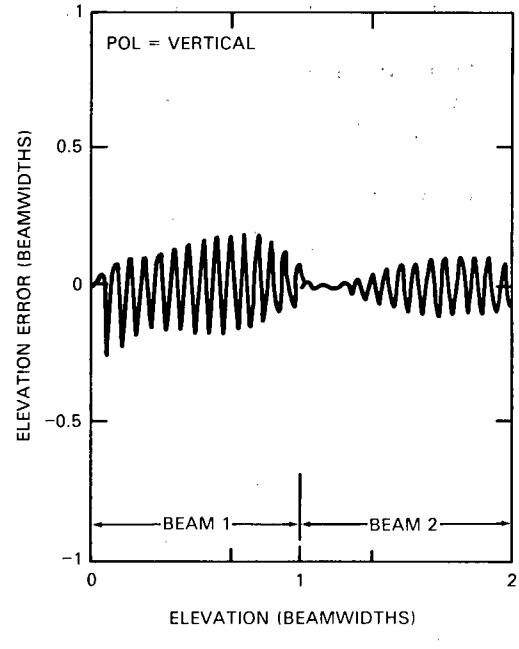

(d) Vertical polarization

Fig. 4 — Azimuth and elevation errors as a function of elevation for $R = 0, P = 0, \mathscr{A} = 90^\circ, \mathscr{B} = 0$, $a_p = 90^\circ$, $e_{p_0} = 1/2$ and 3/2 beamwidths, $D = 3$ m, $d = 9$ m, antenna height = 26 m and target azimuth = 90°.

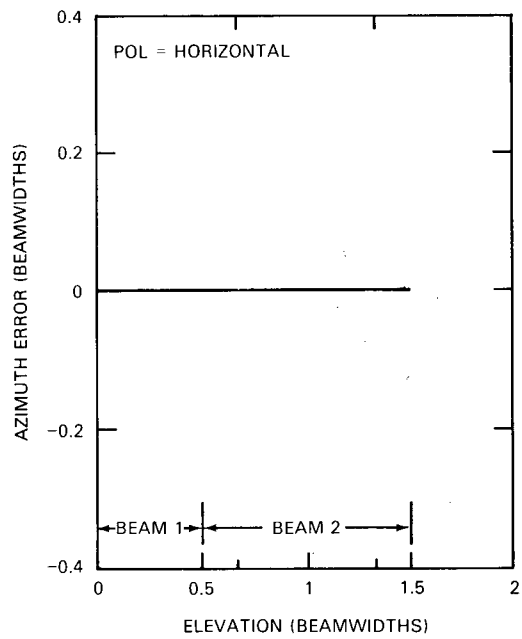

(a) Horizontal polarization

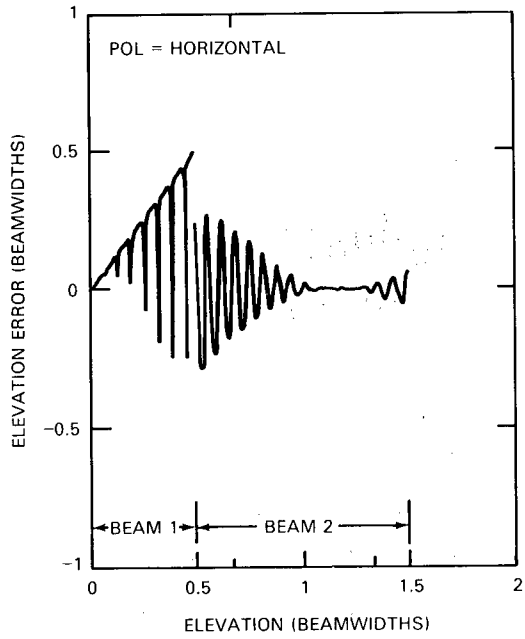

(b) Horizontal polarization

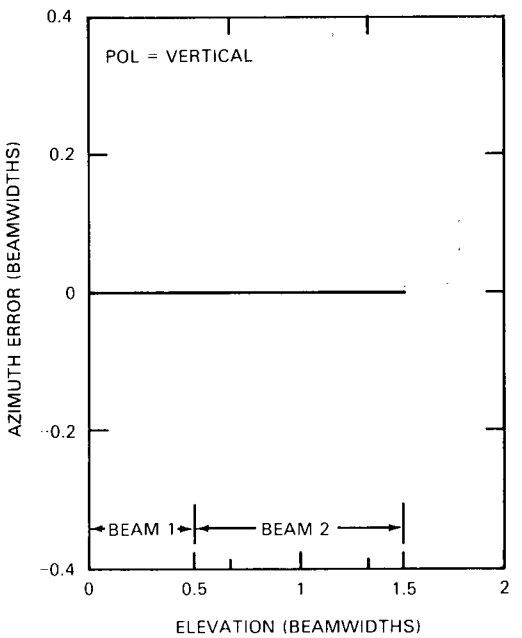

(c) Vertical polarization

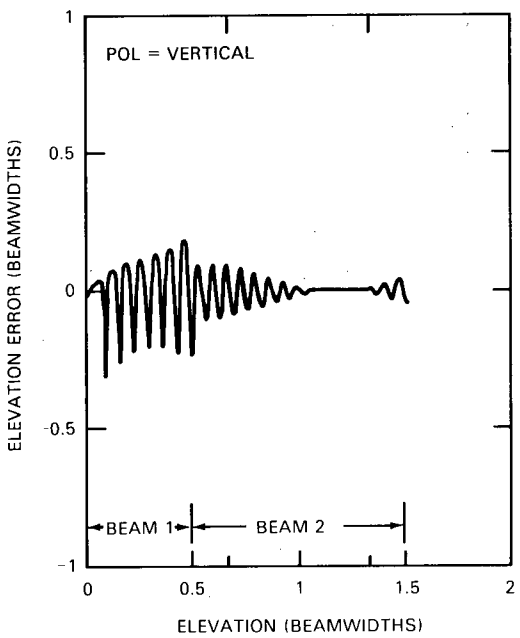

(d) Vertical polarization

Fig. 5 — Azimuth and elevation errors for R = 0, P = 0, $\mathscr{A}$ = 90°, $\mathscr{B}$ = 0, a_p = 90°, e_{p_o} = 0 and 1 beamwidth, D = 3 m, d = 9 m, antenna height = 26 m, and target azimuth = 90°

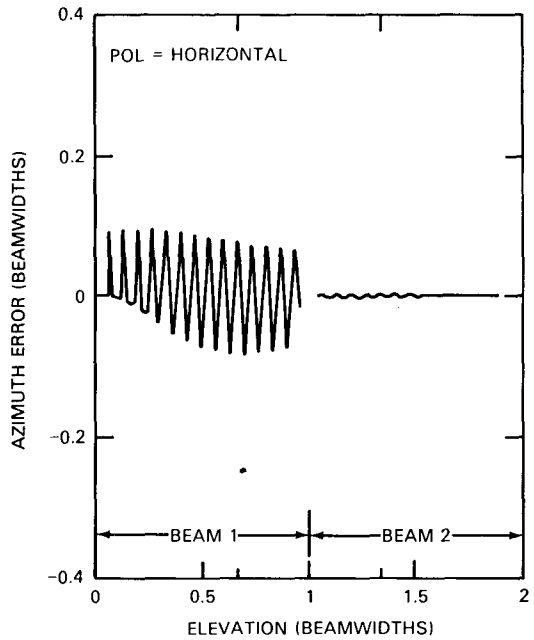

(a) Horizontal polarization

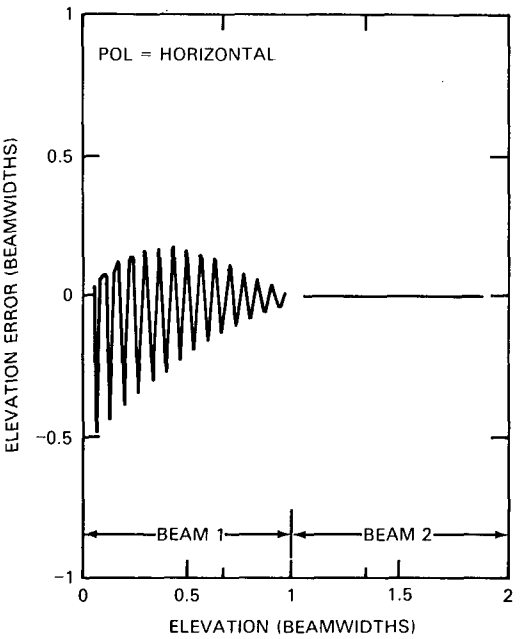

(b) Horizontal polarization

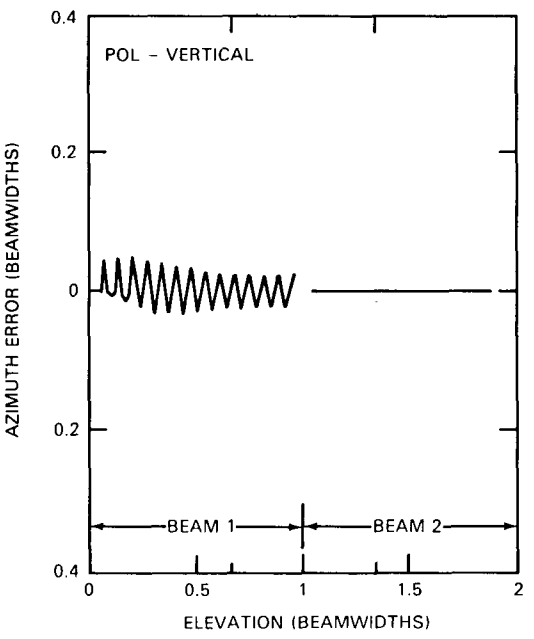

(c) Vertical polarization

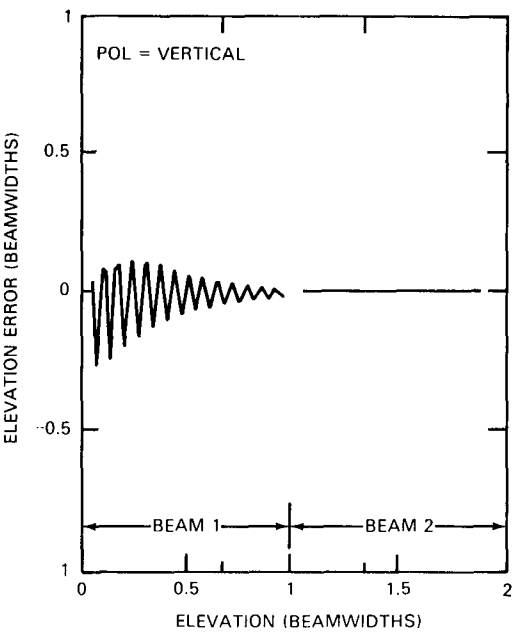

(d) Vertical polarization

Fig. 6 — Azimuth and elevation errors for R = 0, P = 20°, $\mathscr{A}$ = 90°, $\mathscr{B}$ = 0, a_p = 90°, e_p = 1/2 and 3/2 beamwidths, D = 3 m, d = 9 m, antenna height = 26 m, and target azimuth = 90°

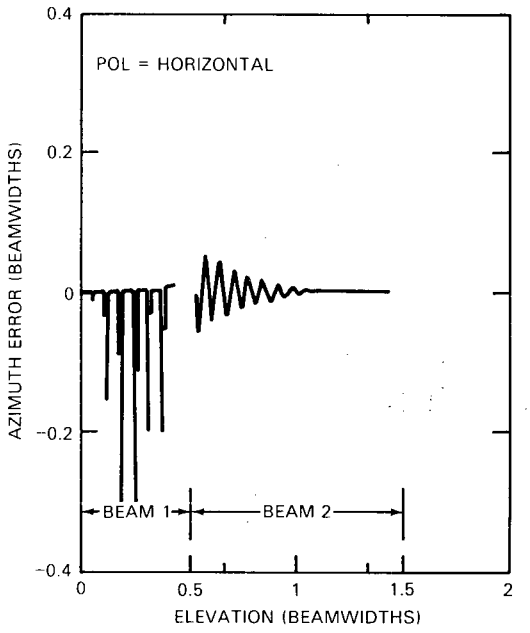

(a) Horizontal polarization

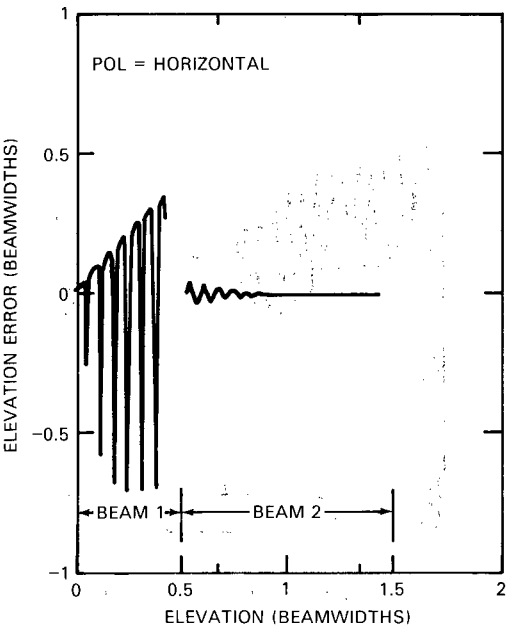

(b) Horizontal polarization

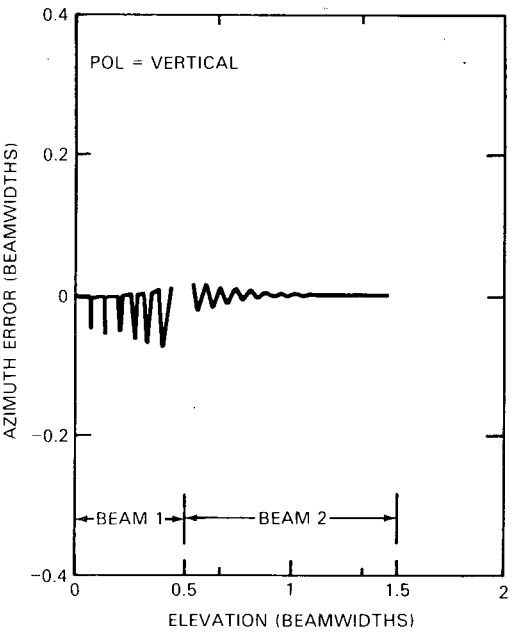

(c) Vertical polarization

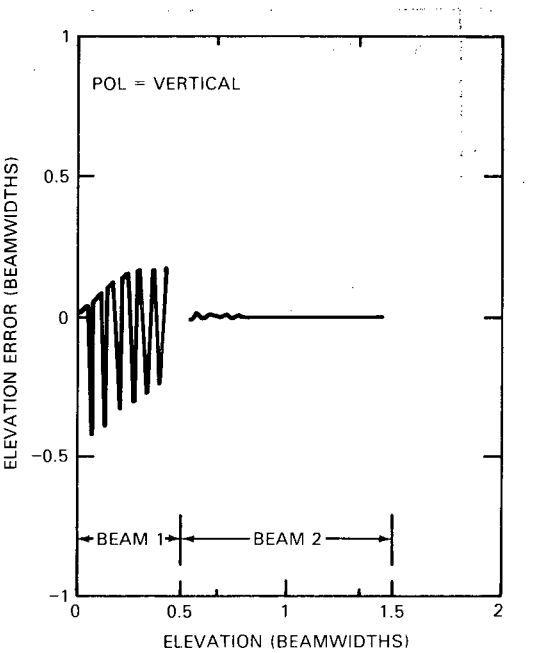

(d) Vertical polarization

Fig. 7 — Azimuth and elevation errors for R = 0, P = 20°, $\mathscr{A}$ = 90°, $\mathscr{B}$ = 0, a_p = 90°, e_p = 0 and 1 beamwidth, D = 3 m, d = 9 m, antenna height = 26 m, and target azimuth = 90°

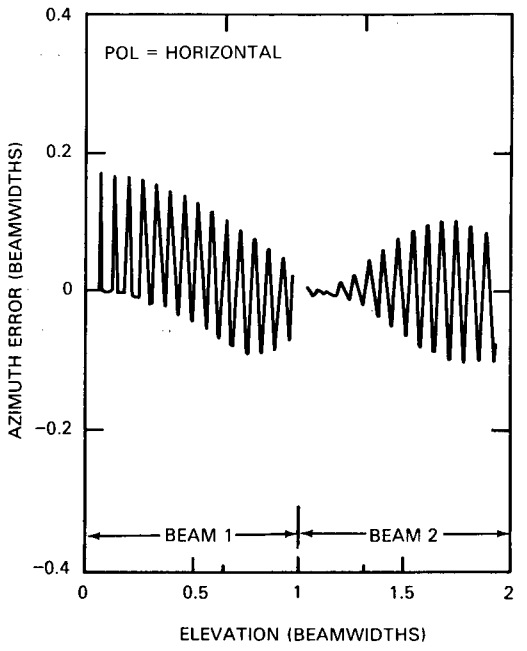

(a) Horizontal polarization

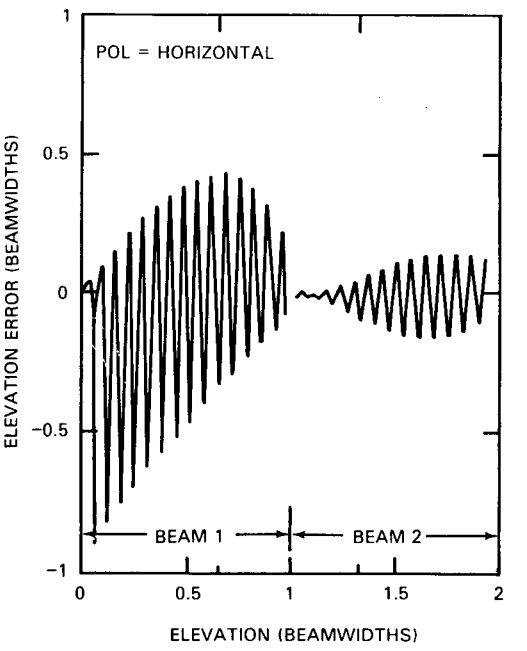

(b) Horizontal polarization

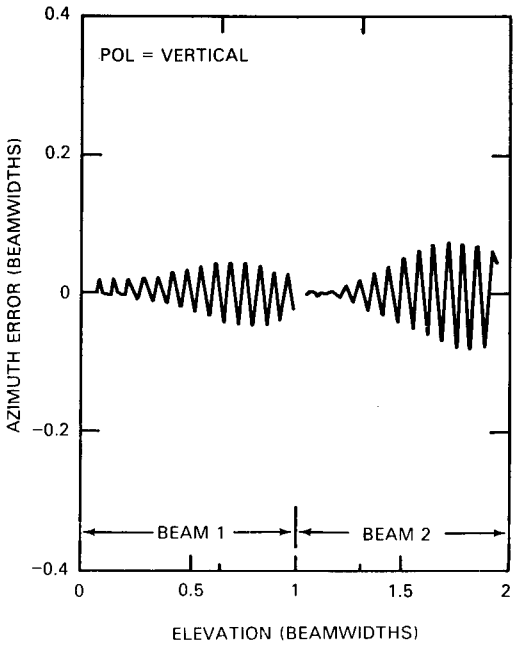

(c) Vertical polarization

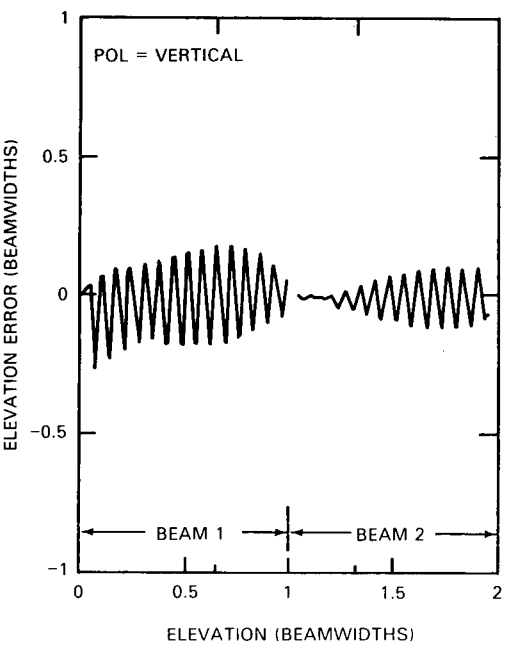

(d) Vertical polarization

Fig. 8 — Azimuth and elevation errors for $R = 0$, $P = 0$, $\mathscr{A} = 90^\circ$, $\mathscr{B} = 0$, $a_p = 45^\circ$ (scanned off axis -45°), e_p = 1/2 and 3/2 beamwidths, D = 3 m, d = 9 m, antenna height = 255 m, and target azimuth = 45°

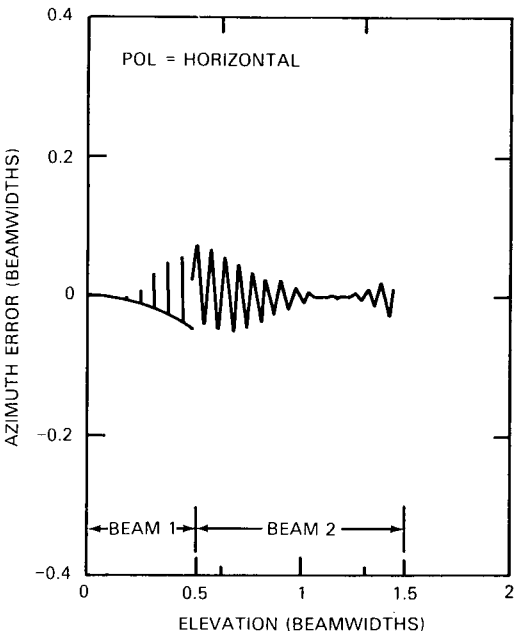

(a) Horizontal polarization

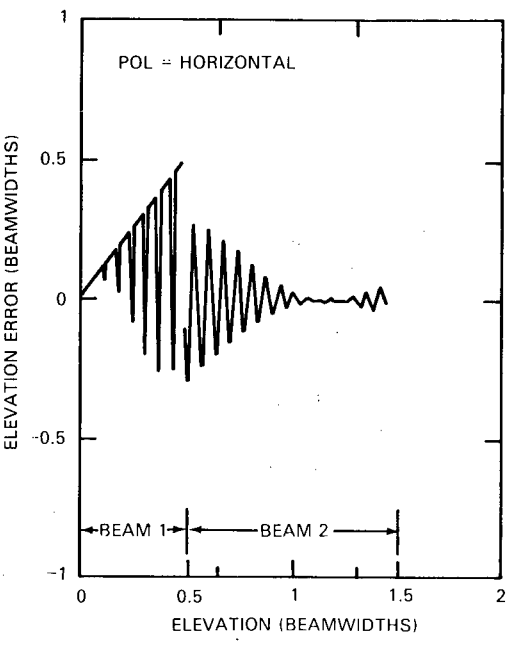

(b) Horizontal polarization

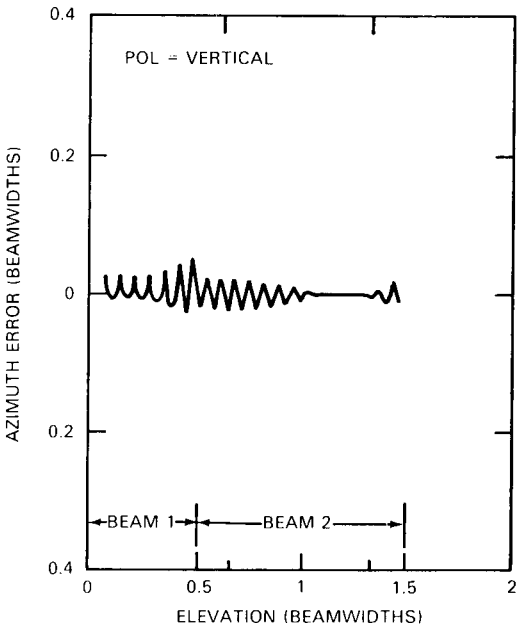

(c) Vertical polarization

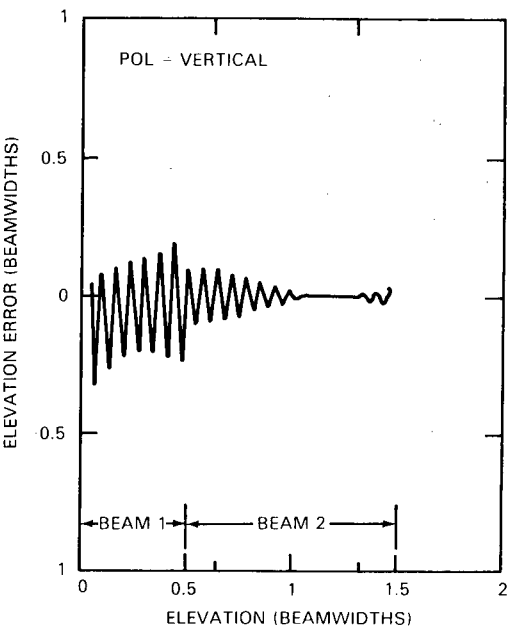

(d) Vertical polarization

Fig. 9 — Azimuth and elevation errors for R = 0, P = 0, $\mathscr{A}$ = 90°, $\mathscr{B}$ = 0, a_p = 45° (scanned off axis −45°), e_p = 0 and 1 beamwidth, D = 3 m, d = 9 m, antenna height = 26 m, and target azimuth = 45°

The azimuth errors were fairly insensitive in terms of beamwidth when the elevation beamwidth was varied until the beamwidth became large. Then the azimuth errors grew rapidly with increasing beamwidth due to coning and multipath. For a UHF array this point occurred for antenna vertical dimensions of slightly below 3 m.

The azmith errors were fairly insensitive in terms of beamwidth when the azimuth beamwidth was varied. Consequently the azimuth error could be decreased by simply constructing a narrower beam in azimuth. The best results are when the beam is nearly circular. These results were confirmed for azimuth beamwidths taken to be equal to up to 1/3 the elevation beamwidths.

When the antenna is crossleveled and at the same time it is scanned off axis, the errors remain commensurate to the errors under each condition by itself. In some cases the error is smaller. For example, when the error due to coning (scanning off axis) is larger than the crosslevel-derived error, the combination of the two requires less scanning off axis to obtain the described pointing angle and consequently has less azimuth error. No conclusions were drawn concerning the effects of polarization. Vertical polarization gave less angle errors in both azimuth and elevation, primarily due to the lower reflection coefficient. However, this result is valid for only a smooth sea. For rough seas the reflection coefficient becomes time varying and, at least on the average, drops in magnitude. No good sea-reflected forward-scatter data exist from which to draw polarization-study conclusions. In general the polarization which yields the lowest reflection coefficient will yield the lowest monopulse angle errors.

Where to point the beam is left unresolved. The error is less in peak magnitude and changes rather smoothly as the target raises in elevation when the beam is pointed up so its 3-dB point is on the water. However, when the beam is straight out on the water, the error is small in azimuth except for sharp spikes which occur when the target and image are out of phase. One could argue that the signal is almost never detected under this condition or spike errors could be thrown out, so that the errors would be the smallest when the beam is on the surface. However, we will not attempt to justify any preferred beam-pointing angle.

In general the azimuth errors in the plane of the sea behave as follows. The azimuth error was not larger than 0.1 beamwidth for vertical polarization with the beam pointed up for the worst cases of a 20° crosslevel or a 45° scan off axis. For conditions less than these the error decreased. The azimuth error was no larger than 0.2 beamwidth for horizontal polarization with the beam pointed up for the worst cases of a 20° crosslevel or a 45° scan off axis (if sufficient vertical aperture is present). Again, as conditions less than these were imposed, the error decreased. The azimuth error is quite small except for spike errors (out-of-phase condition) for both vertical and horizontal polarization when the beam is pointed at the sea surface. These conclusions are valid for a variety of cross-level and scanning-off-axis conditions. In summary monopulse angle measurements in a ship's environment can in most cases give azimuth measurements with a mean value of less than 0.1 beamwidth.

ERRORS DUE TO THERMAL NOISE

In this section the azimuth and elevation errors in the plane of the sea are found in terms of the azimuth and elevation errors in array coordinates. The errors in array coordinates can then simply be related to the signal-to-noise ratio. The total error can then be estimated by using the bias error obtained in the previous section and the random errors discussed in this section.

The error in stabilized coordinates in terms of the error in array coordinates is approximated by using the truncated Taylor series expansion

$$\begin{bmatrix} \Delta a_s \\ \Delta e_s \end{bmatrix} = C \begin{bmatrix} \Delta\gamma \\ \Delta\delta \end{bmatrix}, \tag{32}$$

where $\Delta\gamma$ and $\Delta\delta$ are the azimuth and elevation error in array coordinates, Δa_a and Δe_s are the azimuth and elevation errors in the plane-of-the-sea coordinates, and C is a matrix of partial derivatives:

$$C = \begin{bmatrix} \dfrac{\partial a_s}{\partial\gamma} & \dfrac{\partial a_s}{\partial\delta} \\ \dfrac{\partial e_s}{\partial\gamma} & \dfrac{\partial e_s}{\partial\delta} \end{bmatrix}. \tag{33}$$

The covariance matrix of the errors is then

$$\operatorname{cov}\begin{bmatrix} a_s \\ e_s \end{bmatrix} = C \left[\operatorname{cov}\begin{bmatrix} \gamma \\ \delta \end{bmatrix} \right] C', \tag{34}$$

where cov stands for covariance of the vector, which is a matrix. The covariance matrix in array coordinates is diagonal, and the variances are a function of signal-to-noise ratio. In the examples the standard deviations in γ and in δ are taken to be 0.1 beamwidth. The matrix C is given in Appendix B.

The errors in the plane of the sea are plotted in Figs. 10, 11, and 12 with Figs. 10a, 11a, and 12a being the azimuth errors and Figs. 10b, 11b, and 12b being the elevation errors for a number of different conditions. The target azimuth relative to the array center in plane of the sea coordinates is the abscissa, and the errors are plotted for given elevations in the plane of the sea. From these curves several basic conclusions can be drawn. The elevation errors in the plane of the sea are nearly independent of target position and ship motion. The azimuth error depends on the accuracy of the elevation and azimuth measurements at the array face, the target position with respect to the array, and crosslevel conditions. It appears to be nearly independent of level changes. The azimuth error increases with

target elevation and the amount scanned off axis in azimuth. In other words the more severe the coning, the larger the azimuth error in the plane of the sea. Finally it appears that the azimuth errors in the plane of sea can be held to less than twice the angle-measurement error that is due to thermal noise at the array face.

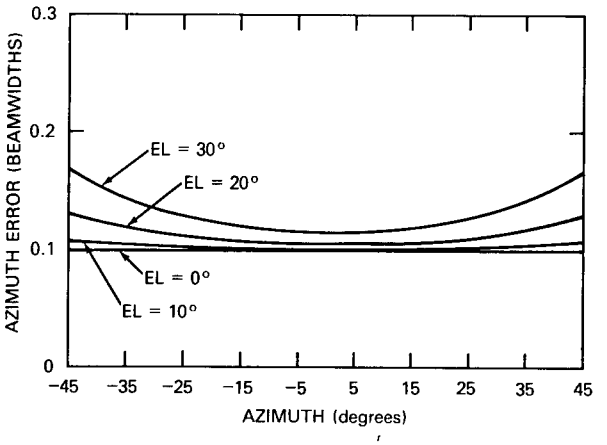

(a) Azimuth errors

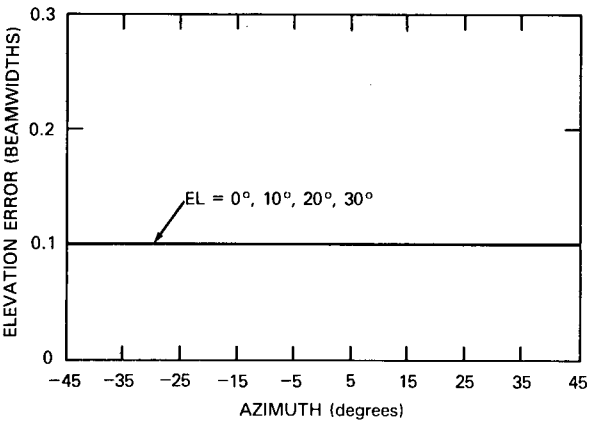

(b) Elevation errors

Fig. 10 — Azimuth and elevation errors in the plane of the sea as a function of the beam scanning off axis in azimuth and elevation. The conditions are R = 0, P = 0, D = 3 m, d = 9 m, and 0.1 beamwidth errors in array coordinates.

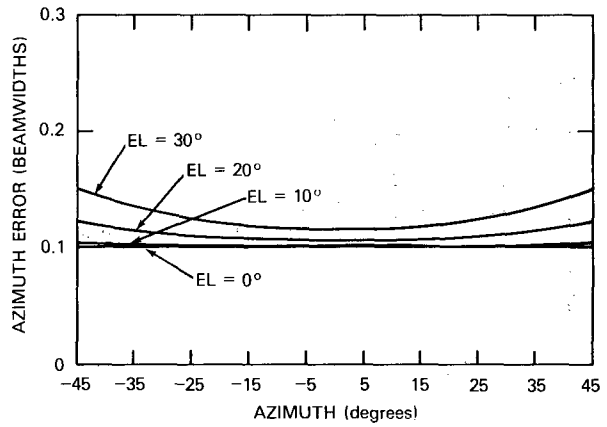

(a) Azimuth errors

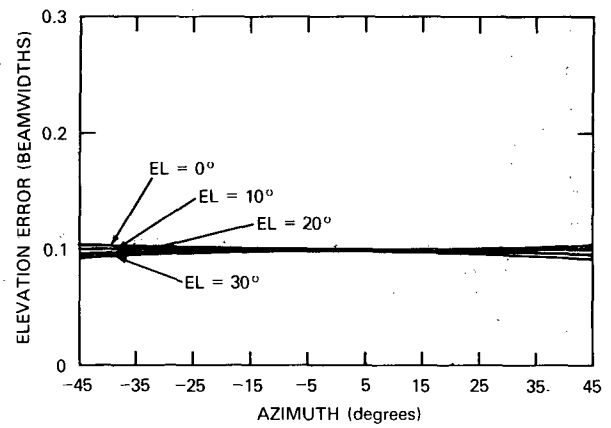

(b) Elevation errors

Fig. 11 — Azimuth and elevation errors in the plane of the sea as a function of the beam scanning off axis in azimuth and elevation. The conditions are $R = 20^{\circ}$, $P = 0$, $D = 3$ m, $d = 9$ m, and 0.1 beamwidth errors in array coordinates.

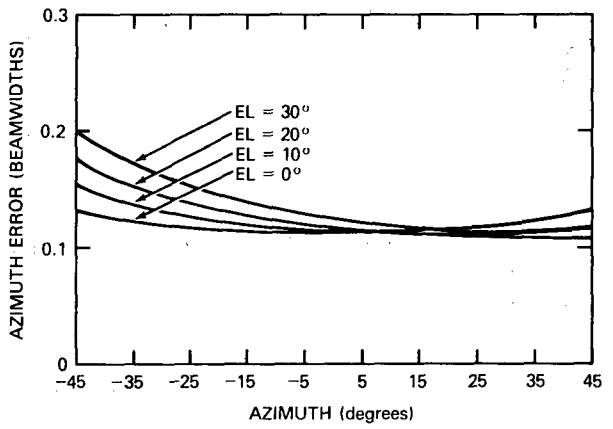

(a) Azimuth errors

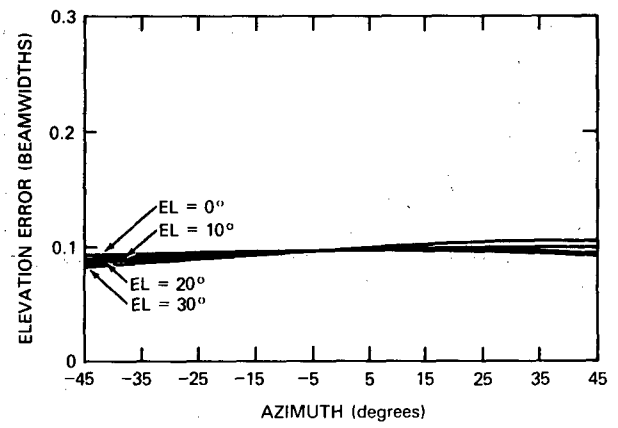

(b) Elevation errors

Fig. 12 — Azimuth and elevation errors in the plane of the sea as a function of the beam scanning off axis in azimuth and elevation. The conditions are R = 0, P = 20°, D = 3 m, d = 9 m, and 0.1 beamwidth errors in array coordinates.

SUMMARY

The errors in shipboard monopulse radars were studied. Of most concern was the azimuth in the plane of the sea. It was found that either or both crosslevel or scanning off axis primarily coupled the multipath-induced errors into the azimuth estimate in the plane of the sea. However, it was also found that the errors in azimuth in the plane of the sea were tolerable, even though the estimates in the antenna coordinates might be quite corrupted. One would probably be able to hold the bias errors in the plane of the sea to less than 0.1 beamwidth. The random errors in azimuth appear to be nearly the same as the errors at the array face except when an antenna is scanned considerably off axis. In the worst case of interest the random errors were no more than twice the random errors at the antenna.

This report does not consider the radar operating in a surveillance mode. To properly study the errors for a surveillance mode, the beam-position algorithm must be defined and the error resulting from measurements in several adjacent beam position on the same target must be incorporated into the analysis.

Appendix A

REFLECTION COEFFICIENT

The reflection coefficients for a smooth sea are

$$\rho_h = \frac{\sin e_s - \sqrt{\epsilon_c - \cos^2 e_s}}{\sin e_s + \sqrt{\epsilon_c - \cos^2 e_s}} \tag{A1}$$

and

$$\rho_v = \frac{\epsilon_c \sin e_s - \sqrt{\epsilon_c - \cos^2 e_s}}{\epsilon_c \sin e_s + \sqrt{\epsilon_c - \cos^2 e_s}}, \tag{A2}$$

where ρ_h and ρ_v are the complex reflection coefficients for horizontal and vertical polarization respectively, e_s is the target elevation angle, and ϵ_c is the complex dielectric coefficient, with $\epsilon_c = \epsilon_1 - j60\lambda\sigma$, in which ϵ_1 is the sea dielectric coefficient, λ is the radiation wavelength, and σ is the sea conductivity. The values used for ϵ_1 and σ are as follows:

Frequency f (MHz)	Dielectric Constant ϵ_1 (F/m)	Conductivity σ (mhos/m)
<1500	80	4.3
1500 to 3000	80 - 0.00733(f - 1500)	4.3 + 0.00148(f - 1500)
3000 to 10,000	69 - 0.00243(f - 3000)	6.52 + 0.001314(f - 3000)

These formulas are given in NRL Report 7098 (L. V. Blake, "Machine Plotting of Radio/Radar Vertical-Plane Coverage Diagrams," June 25, 1970).

To account for the polarization change due to the array crosslevel, the formula for the sum channel becomes

$$\Sigma = \Sigma_h \cos \psi + \Sigma_v \sin \psi, \tag{A3}$$

where Σ_h and Σ_v is the sum-channel signal with horizontal and vertical polarization respectively, ψ is the crosslevel angle, and the array is polarized to receive horizontal polarization. The sum channel for an array being vertical polarized is

$$\Sigma = \Sigma_v \cos \psi + \Sigma_h \sin \psi. \tag{A4}$$

The signals Σv and Σ_h are computed by using (19), with the reflection coefficient being ρ_v or ρ_h, given by (A1) or (A2) respectively. This assumes that target does not depolarize the transmitted signal, which may not be realistic but which was assumed in the examples.

The two difference signals are modified for polarization in the same manner as the sum channel. The crosslevel angle ψ is

$$\psi = \tan^{-1} c_1/c_2, \tag{A5}$$

where

$$c_1 = \sin R \cos P \cos \mathscr{A} + \sin P \sin \mathscr{A}$$

and

$$c_2 = -\sin \mathscr{B}(\sin R \cos P \sin \mathscr{A} - \sin P \cos \mathscr{A}) + \cos R \cos P \cos \mathscr{B}.$$

Appendix B

COEFFICIENTS FOR COVARIANCE CALCULATIONS

The partial derivatives for equation (33) can be written in the form of a product of matrices as

$$C = F\,E\,G\,H, \tag{B1}$$

where the matrices are

$$F = \begin{bmatrix} \cos a_s/\cos e_s & -\sin a_s/\cos e_s & 0 \\ 0 & 0 & 1/\cos e_s \end{bmatrix},$$

$$E = \begin{bmatrix} \cos R & 0 & -\sin R \\ \sin R \sin P & \cos P & \cos R \sin P \\ \sin R \cos P & -\sin P & \cos R \cos P \end{bmatrix},$$

$$G = \begin{bmatrix} \cos \mathscr{A} & \sin \mathscr{A} \cos \mathscr{B} & -\sin \mathscr{A} \sin \mathscr{B} \\ -\sin \mathscr{A} & \cos \mathscr{A} \cos \mathscr{B} & -\cos \mathscr{A} \sin \mathscr{B} \\ 0 & \sin \mathscr{B} & \cos \mathscr{B} \end{bmatrix},$$

and

$$H = \begin{bmatrix} \cos \gamma & 0 \\ \dfrac{-\sin \gamma \cos \gamma}{\cos^2 \delta - \sin^2 \gamma} & \dfrac{-\sin \gamma \cos \delta}{\cos^2 \delta - \sin^2 \gamma} \\ 0 & \cos \delta \end{bmatrix}.$$